physica status solidi pss www.pss-b.com

Molecular Beam Epitaxy Growth of Large-Area GaN/AlN 2D Hole Gas Heterostructures

Reet Chaudhuri, Samuel James Bader, Zhen Chen, David Muller, Huili Grace Xing, and Debdeep Jena*

Large-area growth of polarization-induced 2D hole gases (2DHGs) in a GaN/AlN heterostructure using molecular beam epitaxy (MBE) is demonstrated. A study of the effect of metal fluxes and substrate temperature during growth is conducted to optimize the 2DHG transport. These conditions are adopted for the growth on 2 in. wafer substrates. The obtained results represent a step forward towards achieving a GaN/AlN 2DHG platform for high-performance wide-bandgap p-channel field effect transistors (FETs).

1. Introduction

The impurity doping of GaN using magnesium (Mg) for p-type conductivity was one of the key discoveries, leading to the demonstration of white light-emitting diodes (LEDs) which revolutionized the commercial lighting industry.[1] Since then, III-nitride semiconductor transistors have also enabled new applications in commercial radio-frequency (RF) and power electronics industries.[2] These n-channel high-electron-mobility transistors (HEMTs) utilize a polarization-induced 2D electron gas (2DEG) at the metal-polar Al(Ga)N/GaN interface.[3] The difficulties in obtaining high-conductivity hole channels using Mg doping of GaN have restricted the performance of III-nitride p-channel field-effect transistors (p-FETs), which are necessary to enable wide-bandgap power-efficient complementary circuits. Several groups have demonstrated p-channel FETs[4–9] using polarization-induced 2D hole gases (2DHGs) in Mg-doped III-nitride heterostructures.[10] These have also been used to successfully demonstrate monolithic GaN-based complementary metal oxide semiconductor (CMOS) inverter circuits by Chu et al.[11] and Nakajima et al.[12] However, these low-density 2DHGs either suffer from low conductivity or have a parallel electron conduction channel in the heterostructure.

We have recently reported the observation of the long-missing polarization-induced 2DHG at the undoped GaN/AlN interface[13]—the p-type dual of the ubiquitous undoped Al(Ga)N/GaN 2DEG, which has three times a higher conductivity than the previous reported 2DHGs. These high-density holes give us experimental access to the largely unknown transport physics in the valence band of GaN. Technologically, it is a promising platform to enable high-performance p-channel transistors[14,15] toward realizing wide-bandgap complementary circuits. In the previous report,[13] we had demonstrated the growth of these GaN/AlN structures on small pieces less than 1 cm^2 in size. Moving these growths to larger-area wafers will accelerate research and process development efforts, similar to how the wafer-scale uniform growth of the AlGaN/GaN 2DEGs was a step toward enabling a production-suitable process for HEMTs.[16] In this work, we investigate and demonstrate 1) GaN/AlN heterointerface growth conditions for improved 2DHG transport, leading to 2) controlled 2DHG growths on large areas—quarter of a 2 in. wafer and eventually a full 2 in. wafer.

2. Growth and Methods

The GaN/AlN heterostructures studied in this work were grown in a Veeco Gen10 molecular beam epitaxy (MBE) system. Active nitrogen was provided by a Veeco RF plasma source. Standard effusion cells were used for the Ga and Al metal beams. Commercially available metalorganic chemical vapor deposition (MOCVD)-grown semi-insulating Al-rich AlN of ∼1 μm thickness on c-plane sapphire templates from DOWA Electronics Materials Ltd. were used as the starting substrates. They were mounted on 3 in.-lapped Si wafers using molten indium after ultrasonicating for 15 min each in acetone, methanol, and isopropanol. The substrates were outgassed at 200 °C for 7 h in a load-lock chamber and then at 500 °C for 2 h in a prep chamber before growth to ensure a clean, epiready starting surface. The nitrogen plasma power of 400 W at a flowrate of 2 sccm was used

R. Chaudhuri, Prof. H. G. Xing, Prof. D. Jena
Department of Electrical Engineering
Cornell University
Ithaca, NY 14853, USA
E-mail: rtc77@cornell.edu

S. J. Bader, Dr. Z. Chen, Prof. D. Muller
School of Applied Physics and Engineering
Cornell University
Ithaca, NY 14853, USA

Prof. H. G. Xing, Prof. D. Jena
Department of Material Science and Engineering
Cornell University
Ithaca, NY 14853, USA

Prof. D. Muller, Prof. H. G. Xing, Prof. D. Jena
Kavli Institute of Nanoscience
Cornell University
Ithaca, NY 14853, USA

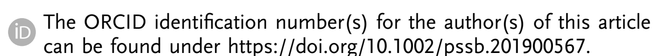
The ORCID identification number(s) for the author(s) of this article can be found under https://doi.org/10.1002/pssb.201900567.

DOI: 10.1002/pssb.201900567

 © 2020 WILEY-VCH Verlag GmbH & Co. KGaA, Weinheim

for the growths, corresponding to a growth rate of ≈520 nm h^{-1}. This was calibrated using the X-ray diffraction (XRD) fitting of a separately grown AlGaN/GaN superlattice (SL) under similar conditions. An AlN buffer of ≈450 nm was grown at a substrate thermocouple temperature of ≈760–790 °C. The initial ≈50 nm of AlN was nucleated and grown under N-rich conditions with Al:N flux ratio <1, and the remaining ≈400 nm was grown in Al-rich conditions with Al:N flux ratio >1. The excess Al accumulated on the surface was consumed periodically using N, as described later. Gallium was used as a surfactant before the Al-rich AlN growth to promote the step-flow mode by enhancing Al-adatom diffusivity.[17] After the AlN growth, the substrate temperature was reduced to 750 °C. The Ga shutter was opened for 10 s to predeposit two monolayers (ML) of Ga on the surface, following which the N shutter was opened, and the unintentionally doped (UID) GaN of required thickness was grown in the Ga-rich intermediate condition. For the growth of Mg-doped InGaN cap layers for the wafers shown in Section 3.2, the substrate temperature was further reduced to ≈680 °C, and the Mg/In/Ga fluxes were adjusted to achieve the desired compositions. Reflection high-energy electron diffraction (RHEED) was used to monitor the surface throughout the growth process. XRD and atomic force microscopy (AFM) were used to characterize the sample post-growth and confirm the targeted heterostructure. Large-area samples were diced, and the sheet resistances of the 2DHGs were then evaluated by Hall effect measurement using soldered corner indium contacts in a Van der Pauw configuration under a 0.32 T magnetic field.

3. Results and Discussions

The III-nitride semiconductors GaN, AlN, and InN possess large spontaneous and piezoelectric polarization arising from the broken inversion symmetry along [0001] or *c*-axis in their wurtzite crystal structures.[3] The polarization difference across a heterointerface consisting of these materials or their alloys gives rise to negative or positive sheet charges at the interface $[(P_{sp}^{Top} + P_{pz}^{Top}) - (P_{sp}^{Bottom} + P_{pz}^{Bottom})] \cdot \hat{n} = \sigma_\pi$, depending on the polarity and structure. Carefully engineered epitaxial heterostructures can, therefore, be grown to achieve desired electronic properties enabled by polarization. In a pseudomorphically grown metal-polar GaN-on-AlN heterostructure, a "negative" polarization sheet charge $\sigma_\pi \sim 5 \times 10^{13}$ cm^{-2} is induced at the GaN/AlN interface due to the large polarization difference. If the top GaN layer is grown thicker than a certain critical value, these negative immobile interface charges should induce positively charged mobile carriers, or holes, confined by the valence band offset between GaN and AlN. No p-type doping is necessary to obtain the high-density 2D holes in the GaN "channel," far exceeding that obtained by impurity doping. This is analogous to the 2DEG in an Al(Ga)N/GaN heterostructure. In a previous work,[13] we reported the observation of this undoped GaN/AlN 2DHG with one of the highest hole densities seen across all material systems and sheet resistances ranging from ∼6–10 kΩ sq^{-1}, a 3× improvement in room-temperature conductivity over previous doped 2DHGs.[15] We next analyze the effect of the growth conditions on the resultant 2DHG channel, identify the optimum condition, and show that large-area 2DHG wafers can be obtained.

3.1. Optimizing the GaN/AlN Interface

A series of samples with ≈13 nm UID GaN/AlN were grown at various substrate temperatures and metal fluxes. The growths were first carried out on 8 × 8 mm^2 pieces of the starting substrate, mounted at the center of a 3 in. Si-lapped wafer to prevent unintentional variation in fluxes from the measured beam equivalent pressure (BEP) before each growth. The samples were rotated at 20 rotations per minute (rpm) during growth.

By keeping the growth conditions of the AlN layer constant, we observed that Ga flux used for the growth of the top UID GaN layer had no perceivable effect on the 2DHG conductivity—as long as the Ga:N flux ratio was > 1. Even for metal-rich conditions that lead to the formation of Ga droplets, 2DHG conductivity was not affected, and the Ga droplets that remained on the surface after growth could be cleaned off by soaking in HCl.

In contrast, clear trends were observed when the growth conditions of the AlN buffer layer were varied, while keeping the GaN layer growth conditions the same. As significant Al desorption from the growth surface is not expected at the typical growth temperature range of ≈650–790 °C for indium-mounted substrates,[18] Al-rich AlN growth results in accumulation of excess Al metal on the growth surface, causing the resultant RHEED pattern to darken as the growth progresses. This is shown in **Figure 1**b. Al droplets on the AlN surface are undesired as they inhibit the formation of an abrupt GaN/AlN interface. To consume these Al droplets, the N shutter is kept open after a period of AlN growth while monitoring the RHEED brightness. The RHEED intensity slowly increases and saturates, indicating that all of the excess Al droplets have been consumed to form AlN. This cycle of AlN growth followed by Al consumption is repeated to grow the entire AlN buffer. A similar technique has previously been reported for the low-temperature MBE growth of AlN by monitoring laser reflectometry signals.[18] Qualitatively, the amount of excess Al—which is determined by the Al:N flux ratio—can affect the AlN surface morphology. A low density of droplets might lead to incomplete coverage of the surface by AlN, whereas it might not be possible to consume a very high density of Al droplets uniformly. There should then exist an optimum Al:N flux for the smoothest AlN buffer surface and consequently, the sharpest GaN/AlN interface. This should be reflected in the 2DHG transport. Figure 1a shows that it is indeed the case—the 2DHG sheet resistances at both 77 and 300 K show clear statistical minima when plotted versus the Al:N flux ratio and also the substrate temperature, with the best transport seen at T_{sub} =780 °C and an Al:N flux ratio of 1.33. The hole densities in all samples measured are consistent with the expected polarization-induced charge of $\sim 5 \times 10^{13}$ cm^{-2}, and the optimized low sheet resistance is a result of the improved mobilities.

The lowest 2DHG sheet resistances measured were ≈6 kΩ sq^{-1} at 300 K and ≈2 kΩ sq^{-1} at 77 K. These are some of the highest conductivity hole channels reported so far in III-nitrides. We previously reported the temperature-dependent transport of similar 2DHGs,[13] showing that their conductivity increases as the temperature is lowered, down to ≈1 kΩ sq^{-1} at 10 K. In recent reports, Poncé et al.[19] and Bader et al.[20] derived that the 300 K transport of the GaN/AlN 2DHG is dominated by acoustic phonons (AP) scattering. At the low

© 2020 WILEY-VCH Verlag GmbH & Co. KGaA, Weinheim

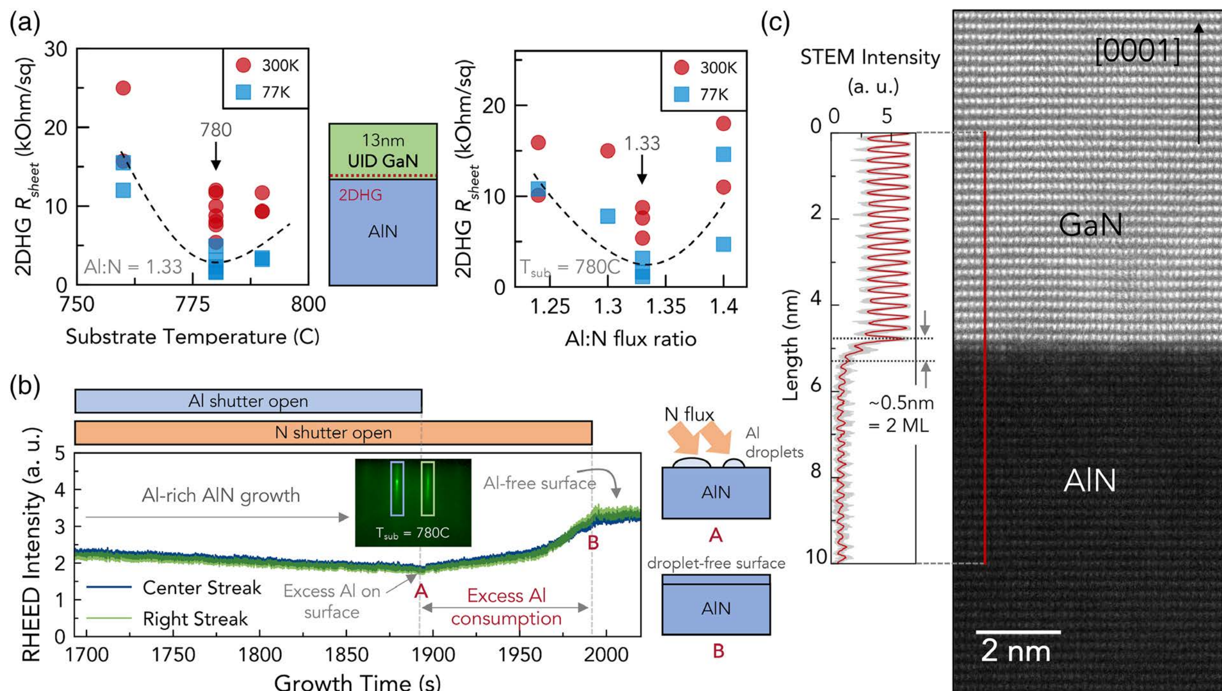

Figure 1. MBE growth of the smooth GaN/AlN interface for high-conductivity 2DHGs. a) Variation in the sheet resistance of the 2DHG structure with AlN buffer grown at different substrate temperatures and Al:N flux ratios. For all samples, the growth condition for the 13 nm UID GaN on top was kept the same. A resistance minimum is observed for both the variables, pointing to an optimum growth condition (dashed lines provided as a guide to the eye). b) RHEED intensity versus growth time, showing the dimming RHEED as excess Al accumulates on the surface during Al-rich AlN growth. The excess Al droplets are then consumed by keeping just the N shutter open after AlN growth. The RHEED intensity brightens and intensity saturates once the excess Al is consumed by N. c) HAADF STEM along the [$\bar{1}$00] zone axis and corresponding line profile of the measured STEM intensity across the GaN/AlN interface. Profiles along 20 lattice lines (gray) are averaged (red), showing a clear intensity difference from the Al and Ga atoms, and the measured heterointerface is ~1–2 ML in thickness.

temperatures of 77 K, phonons freeze out and extrinsic scattering mechanisms such as due to interface roughness (IR) dominate. The AlN/GaN IR has previously been shown to be important for the transport of 2DEG,[21] especially at high charge densities. Similarly, IR scattering likely plays a significant role in the transport at 77 K of the high-density 2DHGs at the GaN/AlN interface. The consumption of excess Al after Al-rich AlN growth at the optimum Al flux (Al:N $\approx$1.33) and substrate temperature (780 °C) is expected to result in a high-quality heterointerface, decreasing the IR scattering and thereby minimizing the 77 K sheet resistances, as shown in Figure 1a.

An atomic-scale image of a GaN/AlN sample grown under optimal conditions was obtained by imaging the interface cross-section in a scanning transmission electron microscope (STEM). Figure 1c shows the high-angle annular dark field (HAADF) STEM image of the GaN/AlN lattice at the interface where the 2DHG is expected. The STEM intensity profile across the interface is plotted. The intensity profile was measured along 20 different lattice lines in the [0001] direction and averaged to highlight the variations. A clear contrast in STEM intensity between Ga and Al atoms is seen due to difference in their atomic numbers. A transition of $\approx$0.5 nm between the Ga and Al atom layer indicates that under the optimized growth condition for 2DHG transport, the GaN/AlN interface is sharp to the order of 1–2 ML.

3.2. Large-Area Growths

The optimum growth conditions for the high-conductivity GaN/AlN 2DHG were then used for growth on larger-area substrates. The structures used for these growths are different from the UID GaN on AlN studied in the previous section by addition of a Mg-doped cap layer of (In)GaN on top of the UID GaN layer, which is desired for low-resistance ohmic contacts to the 2DHG in a p-channel transistor.

Table 1 shows the results of the large-area growths. The heterostructure layer's details of the wafers and the 300 K sheet-resistance maps are shown in **Figure 2**. Wafers B and C have a $\approx$4% InGaN cap on top of the undoped GaN channel

Table 1. Wafer details for large-area growths of GaN/AlN 2DHG structures and corresponding uniformity metrics.

Wafer	Size	Yield [%]	Mean R_{sh} [kΩ sq^{-1}]	Std. Dev. [%]
A	Quarter of 2″	30	21	15.7
B	Quarter of 2″	87.5	10.5	15.8
C	Full 2″ wafer	100	13.3	35.8
			11.4[a)]	20.7[a)]

[a)]Considers only the inner 85% area of the full wafer C.

© 2020 WILEY-VCH Verlag GmbH & Co. KGaA, Weinheim

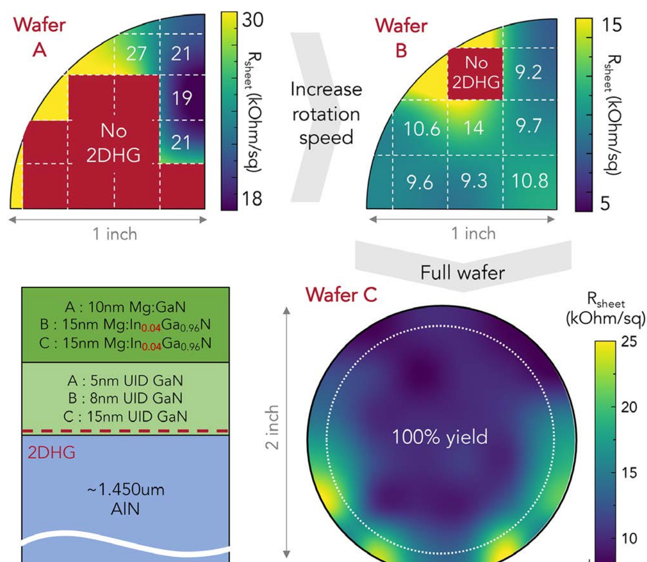

Figure 2. Sheet resistance maps (300 K) of the 2DHG wafers grown using MBE, along with the corresponding heterostructure details. Wafer A was rotated at 20 rpm; wafers B and C were rotated at 30 rpm during growth. The red regions on the maps indicate areas where no 2DHG was measured (high resistance, $R_{sh} > 1\ M\Omega\ sq^{-1}$). The dashed circle inside the full wafer C indicates the area with high-uniform transport.

layer, with targeted Mg-doping densities of $\sim 1 \times 10^{19}$ and $\sim 5 \times 10^{19}\ cm^{-3}$, respectively. The 2DHG sheet densities for each wafer were measured to be approximately uniform across the surface, with varying hole mobilities resulting in sheet resistance distribution. As the three wafers A, B, and C have different structures, we do not compare their sheet resistances. Instead, we focus on the "uniformity" of growth and define the metrics as 1) yield = diced square pieces with a 2DHG/total number of diced square pieces from the wafer and 2) the standard deviation of the sheet resistances as a percentage of the mean. A high yield and a low standard deviation are desirable.

Wafer A was grown on a quarter of a 2 in. substrate wafer using the same growth conditions, as described in Section 3.1; the sample was In mounted on the center of a 3 in.-lapped Si wafer and rotated at 20 rpm (3 s/rotation). As shown in Figure 2, 2DHGs were present in only 4 out of 13 pieces, resulting in a low yield of 30%—indicating nonuniform growth. The growth rate used for this was $520\ nm\ h^{-1}$ or $\approx 1.7\ s\ ML^{-1}$. Thus, at a rotation speed of 20 rpm, the effective growth rate is ≈2 ML per rotation, which could be a possible cause of nonuniformity.

To tackle this, wafer B was grown at an increased rotation speed of 30 rpm corresponding to the effective growth rate of ≈1 ML per rotation, maintaining the rest of the growth conditions identically. An increase in uniformity was observed, with only one piece without a 2DHG, pushing the yield up to 87.5%. Following this result, a third sample—a full 2 in. wafer C—was grown under the same conditions as wafer B. 2DHG conductivity was observed across the whole wafer—a yield of 100%. The lack of carrier freeze-out and increase in their conductivity at 77 K confirmed that the conductivity was due to a 2DHG. Though the standard deviation of sheet resistance is higher for the entire wafer C compared with wafers A/B, if we consider only the inner ≈85% of the wafer surface (dotted circle in Figure 2), the standard deviation decreases to 20.7%. This points to a high uniformity in the central part of wafer C. Further study is necessary to understand nominally higher 2DHG sheet resistances than the small pieces grown under similar conditions.

4. Conclusions

The effects of metal fluxes and substrate temperatures on the transport of the GaN/AlNs 2DHG were studied. Optimal substrate temperature and Al flux were identified to obtain the lowest sheet resistance of 2DHGs. This is believed to be due to the increase in sharpness of the GaN/AlN interface and consequent decrease in IR scattering of 2DHG. The adjustment of the sample rotation speed during growth was found to be essential in obtaining uniform, 2 in. wafer growths of the 2DHG heterostructure. These results make the GaN/AlN 2DHG platform technologically promising and will hopefully accelerate the progress toward high-performance wide-bandgap p-channel FETs.

Acknowledgements

The authors would like to acknowledge funding from Intel, AFOSR (grant AFOSR FA9550-17-1-0048), NSF (grants 1710298 and 1534303), and the Cornell Center for Materials Research from the NSF MRSEC program (DMR1719875). Characterizations and measurements were carried out in part at Cornell NanoScale Facility, an NNCI member supported by NSF (grant ECCS-1542081). The reported data made use of the Cornell Center for Materials Research Shared Facilities, which is supported through the NSF MRSEC program (DMR-1719875) and NSF MRI (DMR-1429155 and DMR-1338010) programs. Z.C. was funded through PARADIM as part of the NSF Materials Innovation Platform program (DMR-1539918).

Conflict of Interest

The authors declare no conflict of interest.

Keywords

molecular beam epitaxy, nitrides, 2D hole gases

Received: September 17, 2019
Revised: December 16, 2019
Published online:

[1] S. Pimputkar, J. S. Speck, S. P. Denbaars, S. Nakamura, *Nat. Photonics* **2009**, *3*, 180.

[2] H. Amano, Y. Baines, E. Beam, M. Borga, T. Bouchet, P. R. Chalker, M. Charles, K. J. Chen, N. Chowdhury, R. Chu, C. De Santi, M. M. De Souza, S. Decoutere, L. Di Cioccio, B. Eckardt, T. Egawa, P. Fay, J. J. Freedsman, L. Guido, O. Häberlen, G. Haynes, T. Heckel, D. Hemakumara, P. Houston, J. Hu, M. Hua, Q. Huang, A. Huang, S. Jiang, H. Kawai, et al., *J. Phys. D: Appl. Phys.* **2018**, *51*, 163001.

 © 2020 WILEY-VCH Verlag GmbH & Co. KGaA, Weinheim

[3] O. Ambacher, J. Smart, J. R. Shealy, N. G. Weimann, K. Chu, M. Murphy, W. J. Schaff, L. F. Eastman, R. Dimitrov, L. Wittmer, M. Stutzmann, W. Rieger, J. Hilsenbeck, *J. Appl. Phys.* **2000**, *87*, 334.
[4] N. Chowdhury, J. Lemettinen, Q. Xie, Y. Zhang, N. S. Rajput, P. Xiang, K. Cheng, S. Suihkonen, H. W. Then, T. Palacios, *IEEE Electron Device Lett.* **2019**, *3106*, 1.
[5] B. Reuters, H. Hahn, A. Pooth, B. Holländer, U. Breuer, M. Heuken, H. Kalisch, A. Vescan, *J. Phys. D: Appl. Phys.* **2014**, *47*, 175103.
[6] H. Hahn, B. Reuters, A. Pooth, B. Hollander, M. Heuken, H. Kalisch, A. Vescan, *IEEE Trans. Electron Devices* **2013**, *60*, 3005.
[7] T. Zimmermann, M. Neuburger, M. Kunze, I. Daumiller, A. Denisenko, A. Dadgar, A. Krost, E. Kohn, *IEEE Electron Device Lett.* **2004**, *25*, 450.
[8] M. Shatalov, G. Simin, J. Zhang, V. Adivarahan, A. Koudymov, R. Pachipulusu, M. A. Khan, *IEEE Electron Device Lett.* **2002**, *23*, 452.
[9] K. Zhang, M. Sumiya, M. Liao, Y. Koide, L. Sang, *Sci. Rep.* **2016**, *6*, 23683.
[10] A. Nakajima, Y. Sumida, M. H. Dhyani, H. Kawai, E. M. S. Narayanan, *Appl. Phys. Express* **2010**, *3*, 121004.
[11] R. Chu, Y. Cao, C. Mary, R. Li, D. Zehnder, *IEEE Electron Device Lett.* **2016**, *37*, 269.
[12] A. Nakajima, S. Kubota, K. Tsutsui, K. Kakushima, H. Wakabayashi, H. Iwai, S. I. Nishizawa, H. Ohashi, *IET Power Electron.* **2018**, *11*, 689.
[13] R. Chaudhuri, S. J. Bader, Z. Chen, D. A. Muller, H. G. Xing, D. Jena, *Science* **2019**, *365*, 1454.
[14] S. J. Bader, R. Chaudhuri, K. Nomoto, A. Hickman, Z. Chen, H. W. Then, D. A. Muller, H. G. Xing, D. Jena, *IEEE Electron Device Lett.* **2018**, *39*, 1848.
[15] G. Li, R. Wang, B. Song, J. Verma, Y. Cao, S. Ganguly, A. Verma, J. Guo, H. G. Xing, D. Jena, *IEEE Electron Device Lett.* **2013**, *34*, 852.
[16] R. Aidam, P. Waltereit, L. Kirste, M. Dammann, R. Quay, *Phys. Status Solidi A* **2010**, *207*, 1450.
[17] A. Nakajima, Y. Furukawa, H. Yokoya, S. Yamaguchi, H. Yonezu, *Jpn. J. Appl. Phys., Part 1* **2006**, *45*, 2422.
[18] V. N. Jmerik, A. M. Mizerov, D. V. Nechaev, P. A. Aseev, A. A. Sitnikova, S. I. Troshkov, P. S. Kop'ev, S. V. Ivanov, *J. Cryst. Growth* **2012**, *354*, 188.
[19] S. Poncé, D. Jena, F. Giustino, *Phys. Rev. Lett.* **2019**, *123*, 096602.
[20] S. J. Bader, R. Chaudhuri, M. F. Schubert, H. W. Then, H. G. Xing, D. Jena, *Appl. Phys. Lett.* **2019**, *114*, 253501.
[21] Y. Cao, K. Wang, G. Li, T. Kosel, H. Xing, D. Jena, *J. Cryst. Growth* **2011**, *323*, 529.

© 2020 WILEY-VCH Verlag GmbH & Co. KGaA, Weinheim